Research Article Vol. 32, No. 4 / 12 Feb 2024 / Optics Express 5353
Optics EXPRESS

All-fiber high-resolution incoherent broadband spectrometer

MARIALUISA CAPEZZUTO,[1,2] DAVIDE D'AMBROSIO,[1,*] ANTONIO GIORGINI,[1] PIETRO MALARA,[1] SAVERIO AVINO,[1] AND GIANLUCA GAGLIARDI[1]

[1]*Consiglio Nazionale delle Ricerche, Istituto Nazionale di Ottica (INO), via Campi Flegrei, 34 - Comprensorio A. Olivetti, 80078 Pozzuoli, Italy*
[2]*Dipartimento di Matematica e Fisica, Università della Campania 'Luigi Vanvitelli', Caserta, Italy*
[*]*davide.dambrosio@ino.cnr.it*

Abstract: Portable optical spectrometers are crucial devices for bio-chemical sensing and spectroscopic applications whereby robust, compact and cost-effective set-ups are desirable. However, existing miniaturized instruments typically struggle to achieve broad wavelength operation and high spectral resolution at the same time. Here, an all-fiber optical spectrometer based on two cascaded Bragg gratings is devised and demonstrated, showing a record resolution and a wavelength span-to-resolution ratio larger than that of most miniature broadband spectrometers reported to date. Thanks to a synchronous control of the grating lengths and to a unique combination of their reflection features, spectral analysis of incoherent light within 1 pm is achieved. On the other hand, fast and reproducible wavelength tuning over several nanometers on a millisecond-timescale is ensured by mechanical stretching of the internal fiber, limited only by the actuator's dynamic range. A striking evidence of the spectrometer capabilities is provided with Doppler-limited spectroscopy of gas absorption bands performed with a near-infrared LED source. The observed spectra exhibit lineshapes comparable with those obtained by laser-based set-ups and the retrieved gas-line parameters are in agreement with existing spectroscopic databases. The spectrometer lends itself to applications in high-resolution interrogation of multiple fiber-optic sensors as well as broadband imaging with supercontinuum light.

1. Introduction

Spectrometers, the most popular instruments to measure optical spectra, analyze the distribution and intensity of absorption, emission and fluorescence features in light transmitted and reflected by various-density media or emitted by radiation sources. They hold a prominent role in biochemistry and spectroscopy laboratories for research and for a wealth of technology applications. In the majority of the cases, spectrometers rely either on scanning interferometers (e.g., fast-Fourier transform devices) or use dispersive elements (e.g., diffraction gratings and prisms) to perform a sequential wavelength filtering [1]. Each set-up yields a different trade-off between operation range, resolution, compactness and speed. Presently, high-performance spectrometers exhibit a wide operation range (hundreds of nanometers or more) but suffer from a limited wavelength resolution and a bulky set-up [2]. In the last years, the miniaturization of optical spectrometers has been a major research trend [3–5]. A particularly useful figure of merit is the span-to-resolution ratio (SRR), i.e. the breadth of the operating window divided by the spectral resolution. Several devices based on micro-electro mechanical systems (MEMS), integrated photonics or optical fiber technology have been demonstrated reaching a SRR in the 10^2-10^3 range [6–8]. This figure can be further improved adopting a different wavelength-selective element as shown in most recent works. Among others, on-chip holographic [9] and metalens-based [10] spectrometers both achieve SRRs exceeding 10^3. An exhaustive overview of the spectral coverage and the resolution of both commercial and research-grade spectrometers can be found in Refs. [3,8].

#505134 https://doi.org/10.1364/OE.505134
Journal © 2024 Received 5 Sep 2023; revised 1 Dec 2023; accepted 3 Dec 2023; published 31 Jan 2024

Optics EXPRESS

Here, we demonstrate a novel concept of broadband optical spectrometer based on the optical filtering of a broadband incoherent source by a special combination of optical fiber Bragg gratings (FBGs) [11]. Our demonstrative set-up, realized entirely with optical-fiber components, delivers a 0.8-pm resolution over a 2-nm spectral band, spanned in ~ 40 ms, thus achieving a SRR > 2000. The overall accessible spectrum limited by the dynamic range of a piezo stretcher and ultimately by the fiber stiffness. The spectrometer performance is experimentally validated carrying out high-resolution absorption spectroscopy of multiple H_2O ro-vibrational transitions with a near-infrared LED.

2. Experimental methodology

The configuration of the high-resolution optical-fiber spectrometer is illustrated in Fig. 1. The core device consists of two FBGs, centered exactly at the same wavelength, one of which presenting a π-phase shifted FBG (PSFBG) structure [12]. If broadband light is coupled to the input fiber and routed to the first FBG via an optical-fiber circulator, the fraction of radiation back-reflected at the Bragg wavelength is directed towards the PSFBG whose transmitted light is the final spectrometer output. The PSFBG exhibits a typical Bragg stopband with 99% reflectivity except for a sharp transmission resonance at the very center. Thus, the resulting spectrum of broadband light initially injected in such system is first reduced to 0.1 nm by the FBG reflection and then filtered down to 0.0008 nm by the narrow transmission feature of the PSFBG.

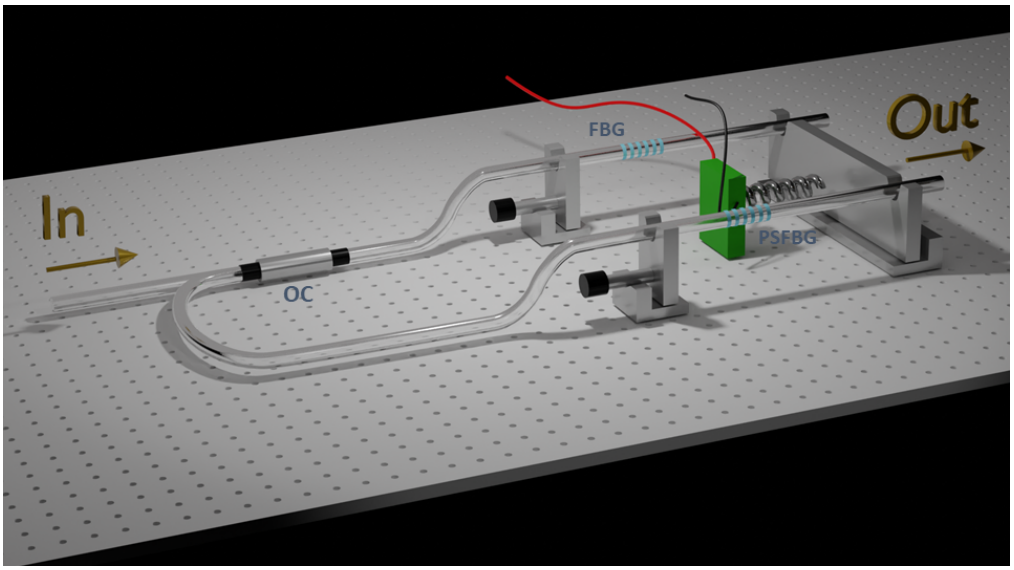

Fig. 1. Setup of the high-resolution optical-fiber spectrometer (OC: optical-fiber circulator).

The spectrometer operation is as follows. The initial spectral alignment for such cascaded filter is attained by two independent micrometric stretching stages. Then, in order to scan the filter position across the broad spectrum of the injected radiation, a strain is applied to both FBGs at the same time, as sketched in Fig. 1, thus shifting their spectral features synchronously by the same amount.

A large, fast and controlled fiber elongation is obtained by means of an amplified piezoelectric (PZT) element mounted inside a flexure housing that acts as a lever arm to amplify the free-stroke displacement of the stand-alone PZT stack (up to ~ 400 μm elongation). In this way, the double FBG system serves as a spectrometer whose center is electrically stretch-tuned within the fiber

Optics EXPRESS

elastic response. The resulting transmission spectrum is shown in Fig. 2 along a wide PZT scan. The temporal response of the fiber stretcher depends on the PZT mount mechanical response (with a resonance around 100 Hz), which results in a minimum duration of ~ 5 ms per each spectral sweep.

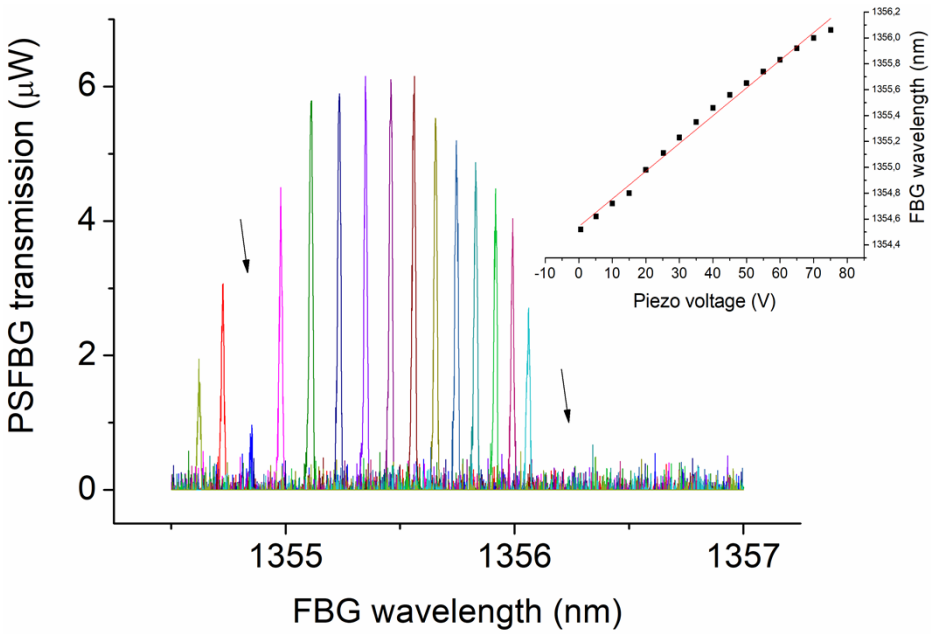

Fig. 2. The filter central feature recorded with the OSA for an increasing voltage applied to the PZT. The black arrows indicate superimposed water vapor absorptions due to ambient air inside the OSA (60-70% humidity). Inset: spectral range of the fiber spectrometer showing a linear response in wavelength (the fit yields a tuning slope of 0.021 ± 0.006 nm/V).

For comparison, in Fig. 3(a), we show the reflection spectrum of the FBG and the transmission spectrum of the PSFBG as seen by an optical spectrum analyzer (OSA) (Ando mod. AQ6317B,

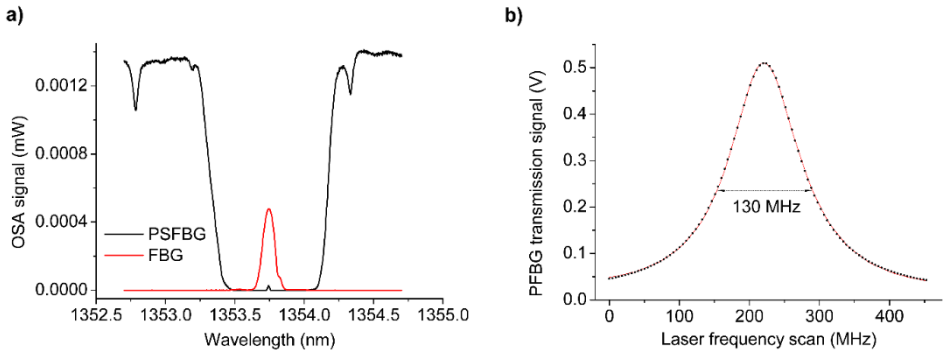

Fig. 3. a) Overlapped reflection spectra of the FBG (red line) and the PSFBG (black line) observed by the OSA around 1353 nm. b) Transmission lineshape of the central PFBG feature as seen along a laser sweep: the lorentzian fit (red line) yields a full width at half maximum of 130 MHz, corresponding to a spectrometer passband of ~ 0.8 pm in wavelength units at 1353 nm.

Optics EXPRESS

resolution 15 pm). The passband of our fiber spectrometer results from the superposition of them, where the PSFBG notch filter is preserved in the cascaded configuration. The spectrometer's resolution cannot be fully appreciated with the OSA, as its sharp transmission feature is 100 times narrower than the instrument resolution. The notch filter spectral feature has a lorentzian lineshape with 130-MHz linewidth, corresponding to a wavelength resolution of 0.8 pm (see Fig. 3(b)).

3. Spectroscopy measurements

We show the spectrometer performance for Doppler-limited absorption spectroscopy of water vapor ro-vibrational transitions belonging to overtone and combination bands near 7380 cm^{-1} (1355 nm in wavelength) using a near-infrared LED. The experimental setup is illustrated in Fig. 4. The incoherent radiation beam from the LED exits to free space through a fiber pig-tailed collimator, passes through the fiber spectrometer and then is directed to a 1-m long absorption cell, equipped with BK7 glass windows and vacuum fittings. The cell transmission is monitored by an InGaAs photodiode. A vacuum pump and a glass flask containing pure liquid water are connected to the cell to extract vapor from a boiling sample and inject it into the cell in a controlled manner. A capacitive manometer is used to measure its pressure while the ambient temperature is maintained around 298 K. In order to provide a wavelength scan over specific regions, a triangular signal is sent to the PZT driver to sweep the spectrometer central wavelength in a continuous way and recover multiple spectral features. Once the spectrometer scan is set around a specific wavelength, the absorption spectra are acquired and analyzed by a fit routine to extract the absorption parameters. To identify the absorption lines from the Hitran database, one can either measure the FBG wavelength shift along the entire scan or calibrate the spectrum by imposing an equivalence between the Doppler linewidth γ_D and the Gaussian full width at half maximum for the lineshape measured for the lowest detectable gas pressure, that for H_2O^{16} is [1]

$$\gamma_D \cong 3.581\ 10^{-7} * v_0 * \sqrt{\frac{T}{M}} \approx 330\ \text{MHz} \tag{1}$$

where V_0 is the line center frequency in cm^{-1}, T the absolute temperature and M is the mass number of the molecule).

In order to recognize the strongest H_2O absorption lines within the LED emission window, we used, in a first instance, a commercial OSA. The observed wideband spectrum is shown in Fig. 5 where two precise regions are selected for deepening our investigation (dotted rectangles).

The first absorption lines observed by the fiber spectrometer are shown in Fig. 6(a). The absorption measurement is made by filling the cell up to ~ 18 Torr, slightly below water vapor saturation at a temperature of 298 K. Here, the voltage offset and amplitude are chosen so that the scan varies in wavenumbers between 7360 cm^{-1} and 7370 cm^{-1}. A 10-cm^{-1} scan with 40-ms duration is sent to the PZT to observe the widest possible spectrum while the cell transmission is detected. The corresponding recording is shown in Fig. 6(b) where a number of strong features with different intensities occur [13]: 7368.8512 cm^{-1} (J = 7 ← 6, Ka = 0 ← 0, Kc = 7 ← 6, 101 vibrational band), 7368.4079 cm^{-1} (J = 7 ← 6, Ka = 1 ← 1, Kc = 7 ← 6, 101 vibrational band), 7366.49012 cm^{-1} (J = 6 ← 5, Kc = 4 ← 3, 101 vibrational band), 7365.0104 cm^{-1} (J = 6 ← 5, Ka = 3 ← 3, Kc = 5 ← 4, 101 vibrational band with two weaker symmetrical lines at 7364.6517 cm^{-1} and 7365.3776 cm^{-1}), and 7361.4760 cm^{-1} (J = 5 ← 4, Ka = 1 ← 1, Kc = 4 ← 3, 101 vibrational band, overlapped with a quasi-degenerate transition at 7361.4802 cm^{-1}). The results show a good agreement of the experimental spectra with the HITRAN database in terms of wavelength positions and linestrength ratios [13].

As a proof of the spectrometer tuning capability, we move the scan center to different wavelengths by rigidly shifting the two FBGs by about 15 cm^{-1}, around 7365 cm^{-1}. The PZT scan is reduced to about 1 cm^{-1} to observe a narrower portion of the spectrum. A triplet of

Optics EXPRESS

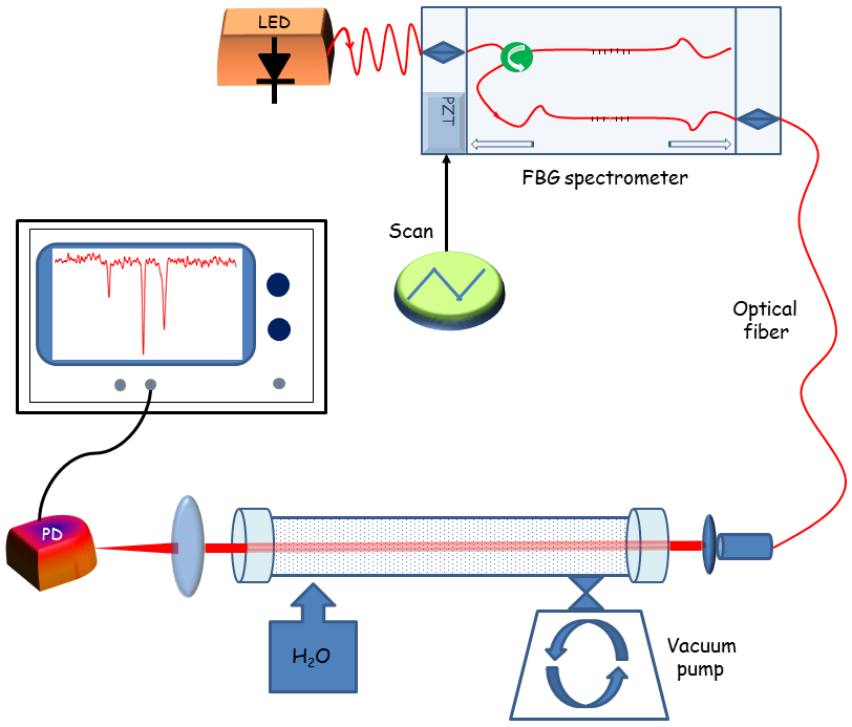

Fig. 4. Optical set-up for spectroscopic measurements (LED: light emitting diode; PD: photodetector)

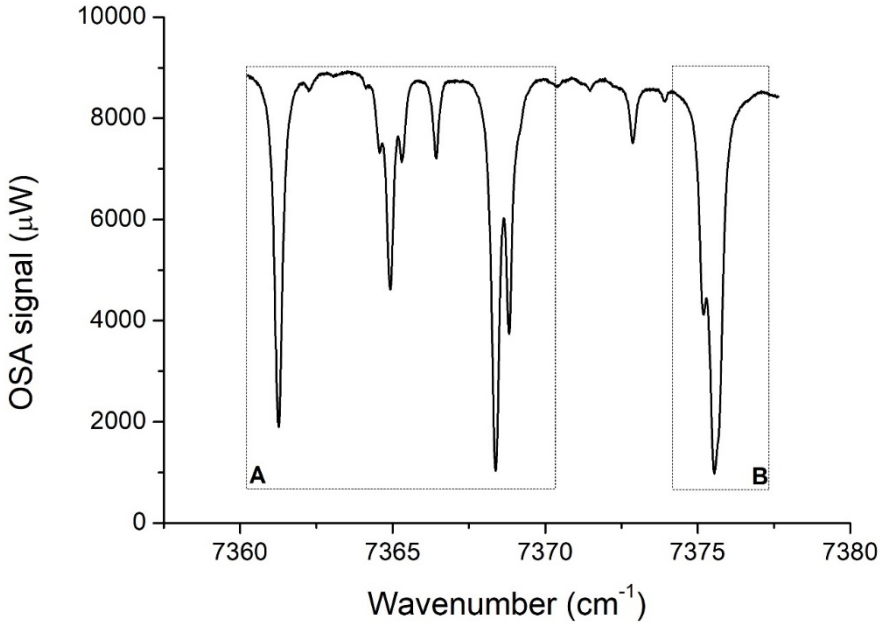

Fig. 5. Wide absorption spectrum recorded by the OSA (at its resolution limit, 15 pm), where the dotted rectangles highlight the spectral regions investigated with the fiber spectrometer.

Optics EXPRESS

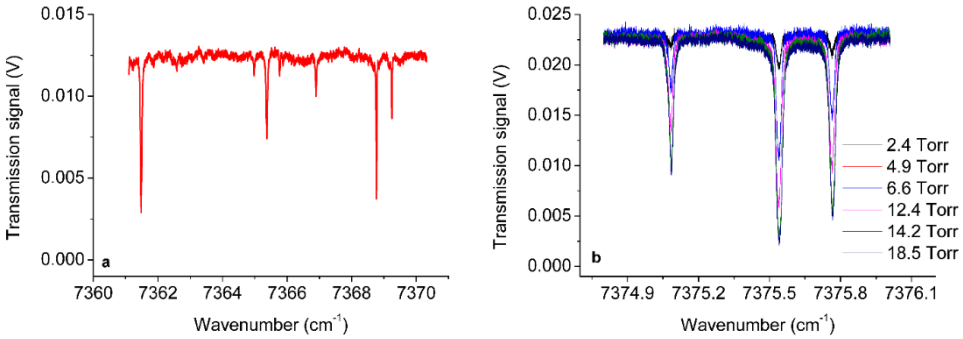

Fig. 6. a) Absorption lineshapes of H2O observed with the fiber spectrometer in region A of Fig. 5 (center wavelength 7365 cm^{-1}, scan range 10 cm^{-1}, scan duration 40 ms; vapor pressure 18.5 Torr). b) Narrower scan over the absorption spectra observed in region B, for different vapor pressure values (center wavelength 7375 cm^{-1}, scan range ~ 1 cm^{-1}; scan duration 40 ms).

strong water vapor lines occurs at wavenumbers $v_1 = 7375.1791$cm-1, $v_2 = 7375.5399\ cm^{-1}$, and $v_3 = 7375.7251\ cm^{-1}$, which correspond to the rotational transition J = 5 ← 4 of the 200 vibrational band, and to the two non-degenerate components of the transition J = 6 ← 5 (Kc = 5 ← 4 & Kc = 3 ← 2) of the 101 vibrational band, respectively. This is shown in Fig. 6(b), where their absorption lineshapes are recorded for different water vapor pressure in the sample cell.

The absorption signals acquired for the strongest line (J = 6 ← 5, Kc = 5 ← 4) in Fig. 6(b) yield the line-center relative absorptions plotted in Fig. 7, over a wide range of pressure values. A low-pressure absorption signal (inset of Fig. 7) is also recorded for wavelength calibration of all spectra, using Eq. (1). From the data shown in Fig. 7, we note the typical saturation behavior expected from the Lambert-Beer absorption law, that is [1]

$$\frac{I}{I_0} = e^{-\alpha p L} \tag{2}$$

being α is the linear absorption coefficient, p the gas pressure and L the optical pathlength (1 m).

As a further assessment of the spectrometer, we directly retrieve the spectroscopic parameters from the spectra recorded in Fig. 5(B). Indeed, the linestrength S is defined as

$$S(T) = \frac{k_B T}{p \cdot L} \int ln\left[\frac{I_0(\nu)}{I(\nu_0)} d\nu\right] \tag{3}$$

where k_B is the Boltzmann constant. For a single absorption line, the integrated absorbance A(p), i.e. the area under the absorption line, can be extracted by a non-linear curve fit (Gaussian profile at low pressure or Lorentian Gaussian fit at low pressure, or a Lorentian profile at high pressure). Thus from Eq. (3), one can write

$$A(p) = \frac{L \cdot S(T) \cdot p}{k_B T} \tag{4}$$

Therefore, the slope B of a linear fit of the A(p) values vs. p yields the linestrength as $S(T) = B \cdot k_B T/L$. The integrated absorbances measured at different pressures for the strongest absorption line at wavenumber $v_2 = 7375.5399\ cm^{-1}$ (Fig. 6(b)) following the above procedure, are shown in Fig. 8. The absorbance data recorded for pressure close to the vapor saturation were not considered to avoid systematic deviations due to water condensation in the sample cell. The linestrength value so extracted with the fiber spectrometer (see Fig. 8 caption) is consistent with that expected from HITRAN database ($S_2^H = 6.8\ 10^{-21}$ cm/molec) [13].

Optics EXPRESS

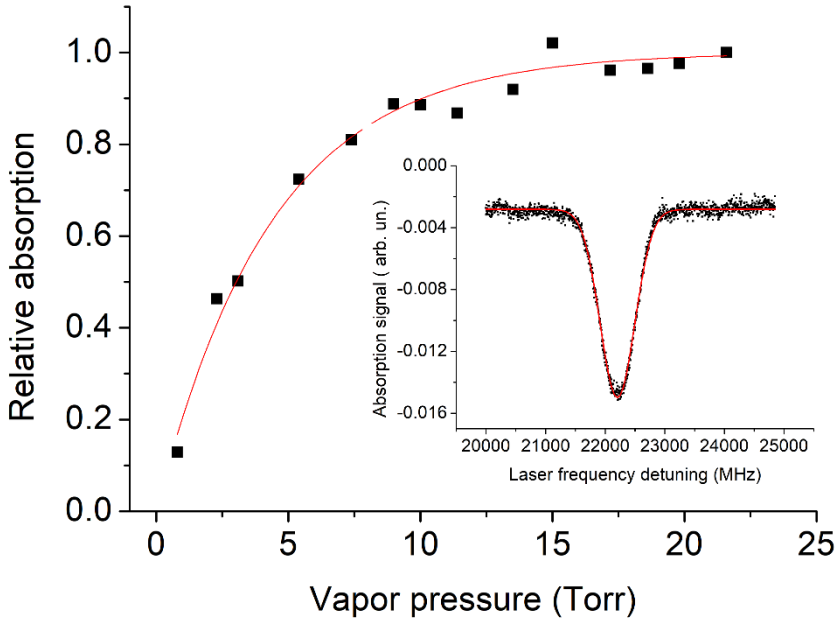

Fig. 7. Lambert-Beer curve retrieved from the spectra recorded for the strongest absorption line in at $v_2 = 7375.5399\,cm^{-1}$ (Fig. 5(B)). Inset: a Gaussian fit of the central absorption line ($7375.5399\,cm^{-1}$) at the lowest pressure (red curve).

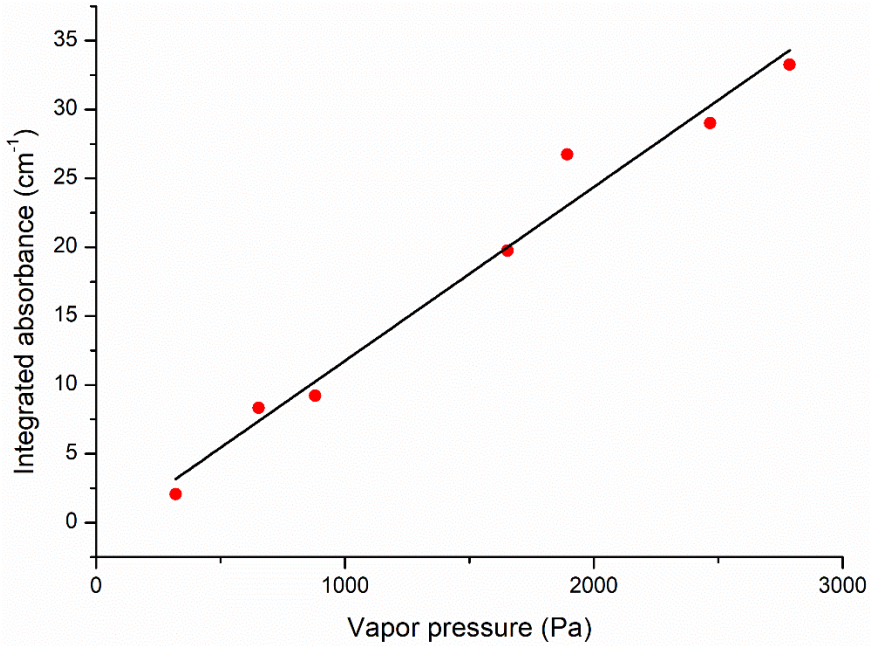

Fig. 8. Linear Fit of the experimental values obtained for the strongest transition. The linestrength measured from the experimental spectra is $S_2 = 6.9 \pm 0.1\ 10^{-21}$ cm/molec.

Optics EXPRESS

4. Conclusions

A new concept of broadband, high-resolution optical-spectrum analyzer entirely based on fiber-optic components is demonstrated. The optical scheme relies on a unique combination of two different types of fiber Bragg gratings that are synchronously wavelength-scanned by an amplified piezoelectric stretcher. Thanks to their small size and high strain sensitivity, the cascaded Bragg filters can sweep several nanometers in a few milliseconds. The system sets a record resolution for all-fiber spectrometers, while preserving a wide wavelength span. Also, this leads to a competitive SRR, inaccessible to many miniaturized devices reported to date [8]. As a proof of concept, we show a direct application to the analysis of absorption spectra observed by a near-infrared LED over a wide range of ro-vibrational transitions belonging to water-vapor overtone bands. The spectrometer operation is suitable to high-resolution interrogation of multiple fiber-optic sensors as well as operation with parallel multiplexed tunable grating filters for ultra-broadband spectroscopy and imaging with supercontinuum light. Although in our demonstrative set-up the scan width is limited to 2 nm by the piezoelectric stretcher, the spectral span actually accessible is ultimately determined by the intrinsic stiffness of the optical fibers in which the FBGs are written. Conventional silica fibers can withstand a 1-% tensile strain [14], which implies that a 10-nm scan is feasible with an appropriate PZT element. However, the use of FBGs written in polymer fibers (e.g., fibers made from PMMA or thermoplastic elastomers (TPEs)), which can be stretched by several times their initial length with only a fraction of the stress needed for silica [15], would enable a much wider spectral window, representing a real step change for the technology presented in this work. The 130-MHz resolution of our spectrometer, already surpassing that of most commercial fiber instruments, such as OSAs and grating spectrometers, is expected to further improve by enclosing the PSFBG filter into a loop resonator. As demonstrated in [16], coupling between the loop and the FBG resonances in such configuration reduces the spectral width of the transmitted radiation by one order of magnitude.

These general concepts envision a new class of miniaturized, low-cost all-fiber optic spectral analyzers with very-high resolution, whereby the use of multiple LEDs and an appropriate choice of photodetectors and fiber-optic components can easily extend the operation to the whole NIR region and to the visible. Their industrial development is possible at costs competitive with existing tunable filter–based microspectrometers harnessing the mass production of the optical fiber elements from the telecommunication market.

Funding. Ministero dell'Università e della Ricerca (20177PSCKT, ARS01_00405, CN 00000023).

Acknowledgments. We thank the colleagues R. Aiello and P. Maddaloni for helpful suggestions and technical support with the vacuum system. This work was partly funded by the Italian Ministry for University and Research (MUR) in the framework of PON project ARS01_00405 OT4CLIMA and Next Generation EU program, Italian Recovery and Resilience Plan (PNRR), MUR - Mission 4, Sustainable Mobility Center CNMS (CN 00000023). Davide D'Ambrosio's fellowship were funded by the Italian Ministry for University & Research (MUR) in the framework of the PRIN2017 PELM project (20177PSCKT grant).

Disclosures. The authors declare no conflicts of interest.

Data availability. Data underlying the results presented in this paper are not publicly available at this time but may be obtained from the authors upon reasonable request.

References

1. *Laser Spectroscopy* (Springer Berlin Heidelberg, 2008).
2. C. Zhu, X. Fu, J. Zhang, *et al.*, "Review of portable near infrared spectrometers: Current status and new techniques," J. Near Infrared Spectrosc. **30**(2), 51–66 (2022).
3. Z. Yang, T. Albrow-Owen, W. Cai, *et al.*, "Miniaturization of optical spectrometers," Science **371**(6528), eabe0722 (2021).
4. H. H. Yoon, H. A. Fernandez, F. Nigmatulin, *et al.*, "Miniaturized spectrometers with a tunable van der Waals junction," Science **378**(6617), 296–299 (2022).
5. Z. Yang, T. Albrow-Owen, H. Cui, *et al.*, "Single-nanowire spectrometers," Science **365**(6457), 1017–1020 (2019).
6. M. Erfan, Y. M. Sabry, M. Sakr, *et al.*, "On-Chip Micro–Electro–Mechanical System Fourier Transform Infrared (MEMS FT-IR) Spectrometer-Based Gas Sensing," Appl. Spectrosc. **70**(5), 897–904 (2016).

Optics EXPRESS

7. O. Manzardo, H. P. Herzig, C. R. Marxer, *et al.*, "Miniaturized time-scanning Fourier transform spectrometer based on silicon technology," Opt. Lett. **24**(23), 1705 (1999).
8. M. Capezzuto, D. D'Ambrosio, S. Avino, *et al.*, "Ultra-broadband high-resolution microdroplet spectrometers for the near infrared," Opt. Lett. **47**(1), 102 (2022).
9. A. Koshelev, G. Calafiore, C. Peroz, *et al.*, "Combination of a spectrometer-on-chip and an array of Young's interferometers for laser spectrum monitoring," Opt. Lett. **39**(19), 5645 (2014).
10. A. Y. Zhu, W.-T. Chen, M. Khorasaninejad, *et al.*, "Ultra-compact visible chiral spectrometer with meta-lenses," APL Photonics **2**(3), 036103 (2017).
11. Y.-J. Rao, "In-fibre Bragg grating sensors," Meas. Sci. Technol. **8**(4), 355–375 (1997).
12. S. Deepa and B. Das, "Interrogation techniques for π-phase-shifted fiber Bragg grating sensor: A review," Sens. Actuators, A **315**, 112215 (2020).
13. I. E. Gordon, L. S. Rothman, R. J. Hargreaves, *et al.*, "The HITRAN2020 molecular spectroscopic database," J. Quant. Spectrosc. Radiat. Transfer **277**, 107949 (2022).
14. L. Yi and Y. Changyuan, "Highly stretchable hybrid silica/polymer optical fiber sensors for large-strain and high-temperature application," Opt. Express **27**(15), 20107 (2019).
15. S. Shabahang, F. Clouser, F. Shabahang, *et al.*, "Single-Mode, 700%-Stretchable, Elastic Optical Fibers Made of Thermoplastic Elastomers," Adv. Opt. Mater. **9**(12), 2100270 (2021).
16. P. Malara, C. E. Campanella, F. De Leonardis, *et al.*, "Enhanced spectral response of π-phase shifted fiber Bragg gratings in closed-loop configuration," Opt. Lett. **40**(9), 2124 (2015).